Journal of The Electrochemical Society, **151** (8) G528-G535 (2004)
0013-4651/2004/151(8)/G528/8/$7.00 © The Electrochemical Society, Inc.

ALD of SiO_2 at Room Temperature Using TEOS and H_2O with NH_3 as the Catalyst

J. D. Ferguson,[a] E. R. Smith,[a] A. W. Weimer,[b] and S. M. George[a,b,z]

[a]*Department of Chemistry and Biochemistry and* [b]*Department of Chemical and Biological Engineering, University of Colorado, Boulder, Colorado 80309, USA*

Amine catalysts can reduce the high temperatures and long exposure times required for SiO_2 atomic layer deposition (ALD) using $SiCl_4$ and H_2O reactants. One problem is that the reaction product, HCl, readily reacts with the amine catalysts to form a salt. Salt formation can be avoided by using organometallic silicon precursors. This study investigated catalyzed SiO_2 ALD on $BaTiO_3$ and ZrO_2 particles using alternating exposures of tetraethoxysilane (TEOS) and H_2O at 300 K with NH_3 as the catalyst. The sequential surface chemistry was monitored in a vacuum chamber using *in situ* transmission Fourier transform infrared (FTIR) spectroscopy. Alternating TEOS/NH_3 and H_2O/NH_3 exposures yielded $Si(OCH_2CH_3)_x$* and SiOH* surface species, respectively, that sequentially deposited silicon and oxygen. Repetition of the TEOS and H_2O exposures in an ABAB... reaction sequence led to the appearance of bulk SiO_2 vibrational modes. The infrared absorbance of these bulk SiO_2 vibrational modes increased with the number of AB reaction cycles. After SiO_2 deposition, the $BaTiO_3$ and ZrO_2 particles were examined using transmission electron microscopy (TEM). The TEM images revealed extremely uniform and conformal SiO_2 films. The measured SiO_2 film thicknesses were consistent with SiO_2 ALD growth rates of 0.7-0.8 Å per AB reaction cycle. The NH_3 catalysis mechanism was also explored by monitoring the FTIR spectra of hydroxylated SiO_2 particles *vs.* NH_3 pressure at constant temperature and *vs.* temperature at constant NH_3 pressure. The spectra revealed strong hydrogen bonding between NH_3 and SiOH* surface species that activates the oxygen in SiOH* for nucleophilic attack. Catalyzed SiO_2 at room temperature should be useful for deposition of inorganic and insulating films on thermally fragile organic, polymeric, or biological substrates.
 [DOI: 10.1149/1.1768548]

Manuscript submitted July 9, 2003; revised manuscript received February 2, 2004. Available electronically July 20, 2004.

The atomic layer controlled growth of conformal thin films can be obtained using atomic layer deposition (ALD) techniques.[1-3] ALD is based on sequential, self-limiting surface reactions. By repeating these sequential reactions, an expanding list of materials can be deposited in reasonable time scales.[3] Deposition of inorganic films on organic, polymeric or biological substrates demands low temperatures, typically less than 100°C. Very few ALD processes can be performed at these low temperature using thermally driven chemistry. One promising approach that has the potential to reduce ALD growth temperature is plasma-assisted ALD.[4]

SiO_2 is an important inorganic material useful in a variety of insulation, protection, and diffusion barrier applications. SiO_2 chemical vapor deposition (CVD) can be achieved using the binary reaction: $SiCl_4 + 2H_2O \rightarrow SiO_2 + 4HCl$.[5] The ALD of SiO_2 can be achieved by breaking the CVD reaction into two separate half-reactions[6,7]

$$(A)\quad SiOH^* + SiCl_4 \rightarrow SiOSiCl_3^* + HCl \qquad [1]$$

$$(B)\quad SiCl^* + H_2O \rightarrow SiOH^* + HCl \qquad [2]$$

where* indicates a surface species. By repeating these reactions in an ABAB... sequence, SiO_2 can be deposited with atomic layer control.[7] These reactions have also been employed to coat boron nitride particles with SiO_2.[8] Unfortunately, SiO_2 ALD using $SiCl_4$ and H_2O has some serious drawbacks such as high required reaction temperatures of 600-800 K, large reactant exposures of $\sim 10^9$ L ($1\ L = 1 \times 10^{-6}$ Torr s), and corrosive HCl as a reaction product.

Amine bases can catalyze the $SiCl_4$ and H_2O reactions during SiO_2 ALD.[9,10] With the amine base catalyst, the reaction requires much smaller reactant exposures of $\sim 10^4$ L and the reaction temperature can be lowered to ~300 K. However, a problem with catalyzed SiO_2 ALD is that the amine catalysts readily react with the HCl reaction product to form a salt. For example, ammonium chloride forms when using NH_3 as the catalyst: $NH_3 + HCl \rightarrow NH_4^+Cl^-$. Similar salt formation is observed during amine-catalyzed chlorosilane attachment on SiO_2 surfaces.[11]

Salt formation could be eliminated by using an organometallic silicon precursor instead of $SiCl_4$. One common silicon organometallic precursor, tetraethoxysilane (TEOS), could be used for SiO_2 ALD based upon the following proposed reaction sequence

$$(A)\quad SiOH^* + Si(OCH_2CH_3)_4 \rightarrow SiOSi(OCH_2CH_3)_3^* + CH_3CH_2OH \qquad [3]$$

$$(B)\quad Si(OCH_2CH_3)^* + H_2O \rightarrow SiOH^* + CH_3CH_2OH \qquad [4]$$

Because CH_3CH_2OH (ethanol) is the reaction product instead of HCl, the salt formation would be avoided because ethanol does not react with NH_3.

The surface half-reactions for ALD are closely related to the overall reaction for the parent CVD process. There are no previous reports of SiO_2 CVD using TEOS and H_2O except with plasma-assisted CVD.[12] Consequently, the reactions given by Eq. 3 and 4 may require high reaction temperatures where TEOS may also pyrolyze to form SiO_2.[13,14] To avoid these high temperatures, SiO_2 ALD could be performed at lower temperatures using an amine base catalyst. Earlier studies of amine-catalyzed alkoxysilane attachment to SiO_2 provide evidence that catalyzed SiO_2 ALD using TEOS and H_2O may be feasible.[15,16]

In this study, Fourier transform infrared (FTIR) spectroscopy was used to monitor the SiO_2 ALD surface chemistry at room temperature during the TEOS and H_2O reactions with NH_3 as the catalyst. FTIR was also employed to monitor the progressive growth of SiO_2 bulk vibrational modes during the AB reaction cycles. Subsequently, SiO_2 films on $BaTiO_3$ and ZrO_2 particles were analyzed using transmission electron microscopy (TEM). These FTIR and TEM studies reveal that conformal and ultrathin SiO_2 films can be deposited at room temperature using sequential reactions of TEOS and H_2O in the presence of the NH_3 catalyst. Additional FTIR investigations explored the catalytic mechanism by focusing on the

[z] E-mail: Steven.George@Colorado.Edu

effect of NH_3 on SiOH* surface species. The FTIR spectra are consistent with strong hydrogen bonding between NH_3 and SiOH* surface species.

Experimental

The $BaTiO_3$ and ZrO_2 particles were coated using SiO_2 ALD in a vacuum apparatus designed for *in situ* transmission FTIR vibrational spectroscopy studies. This vacuum apparatus has previously been described in detail.[8,17,18] FTIR spectroscopy provides an effective way to monitor the surface chemistry occurring during ALD. Transmission FTIR spectroscopy studies require the use of high-surface-area samples. The $BaTiO_3$ particles used in this study were obtained from Ferro Electronic Materials (Penn Yan, New York). These particles were spherical with an average diameter of $\sim$0.5 μm. The ZrO_2 particles were provided by Nanomaterials Research Corporation (Longmont, CO). The ZrO_2 particles were spherical with an average diameter of $\sim$50 nm and a surface area of $\sim$20.2 m^2/g.

TEOS was obtained from Alfa Aesar and had a purity of 99.999+%. The H_2O used was high-pressure liquid chromatography (HPLC) grade from Fisher Scientific. Anhydrous NH_3 (99.99%) from Matheson was employed as the catalyst.

The $BaTiO_3$ and ZrO_2 particles were supported by a tungsten grid. This tungsten grid had 100 lines per inch and was obtained from Buckbee-Mears in St. Paul, MN. The particles were pressed into the grid using polished stainless steel dies and a manual press.[19] A tantalum foil was spot-welded to each side of the grid to facilitate resistive heating. This sample was then suspended between two copper clamps on the sample mount as described previously.[18]

The sample mount was attached to an x-y-z rotary manipulator. The x-y-z adjustment capabilities were useful for proper alignment of the sample in the infrared beam. The manipulator also contained current and thermocouple feedthroughs for sample heating and temperature regulation. The vibrational spectroscopic studies were performed with a Nicolet Magna 560 FTIR spectrometer and MCT-B infrared detector. All of the spectra in this study were recorded with the sample at 300 K. During reactant exposures, the CsI windows on the chamber were isolated by gate valves to prevent deposition on the windows.

The TEM analysis was performed by Dr. Huifang Xu in the Department of Earth and Planetary Sciences and the Center for Composite and Ceramic Materials at the University of New Mexico. The TEM results were obtained with a HRTEM JEOL 2010 high-resolution transmission electron microscope in combination with electron-dispersive spectroscopy and a GATAN digital micrograph with a slow scan CCD camera. These TEM studies monitored the conformality and morphology of the SiO_2 coatings on the $BaTiO_3$ and ZrO_2 particles.

For the FTIR studies of the catalysis mechanism, silica particles from Aldrich with an average diameter of 70 Å and a surface area of 380 m^2/g were pressed into the tungsten grid. Initially, the sample was annealed at 600 K for 5 min and then allowed to cool. The experiments were then performed at 300 K under isothermal conditions. Anhydrous ammonia gas from Aldrich (99.99%) was introduced into the chamber to obtain pressures ranging from 0.02 to 100 Torr. FTIR spectra were recorded at these various NH_3 pressures measured using a Baratron. Experiments were also performed under isobaric conditions. FTIR spectra were recorded for temperatures ranging from 300 to 400 K at a constant NH_3 pressure of 5 Torr.

After these isothermal and isobaric experiments, the sample was moved out of the IR beam. The chamber was then filled with ammonia gas at the same NH_3 pressures utilized in the isothermal and isobaric experiments. The FTIR spectra were recorded to obtain the NH_3 gas-phase features. Subsequently, these spectra were used to subtract the gas-phase features from the composite spectra including both gas and surface species. This subtraction leaves only the absorption features associated with NH_3 adsorbed on the SiO_2 surface.

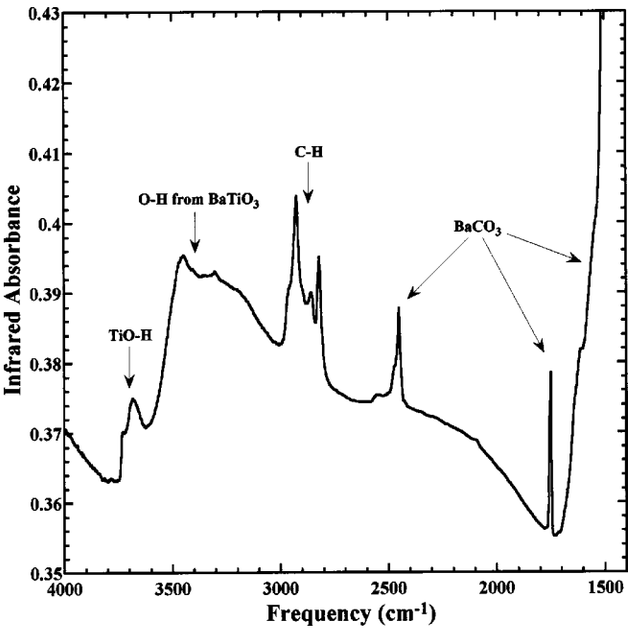

Figure 1. FTIR spectrum of the initial $BaTiO_3$ particles in vacuum at 300 K.

Results and Discussion

Surface chemistry.—The initial surface of the $BaTiO_3$ particles was analyzed using transmission FTIR spectroscopy. After loading the sample in the vacuum chamber, a spectrum of the $BaTiO_3$ particles was recorded at 300 K. The bulk vibrational modes of $BaTiO_3$ lead to strong infrared absorbance below 800 cm^{-1}.[20,21] A pronounced carbonate impurity in the $BaTiO_3$ bulk is also apparent at 1455 cm^{-1}.[20,21] The initial FTIR spectrum referenced relative to the CsI windows is shown in Fig. 1. The FTIR spectrum from 2700 to 4000 cm^{-1} reveals C-H and O-H stretching vibrations.

The absorption feature at 3732 cm^{-1} has the same frequency as the hydroxyl species observed during TiO_2 ALD and may be attributed to TiOH* species.[22] The absorption feature at 3681 cm^{-1} is similar in frequency to hydroxyl species identified as TiOH* surface species on a rutile TiO_2 surface.[23] Other broad absorbance features in the O-H stretching region are observed in the region from 3000 to 3600 cm^{-1}, in agreement with previous studies of $BaTiO_3$ particles.[24] The FTIR spectra also reveal impurities on the surface of the $BaTiO_3$ particles. Features at 1455, 1749, and 2452 cm^{-1} have been assigned to $BaCO_3$ on the surface of $BaTiO_3$.[21] Additional features observed in the range 2800-3000 cm^{-1} are in the C-H stretching region. These absorption features are indicative of hydrocarbon contamination on the surface of the $BaTiO_3$ particles.

The results of the first two AB cycles during SiO_2 ALD are shown in Fig. 2. The FTIR spectra are difference spectra and are displaced from the origin for clarity in presentation. Figure 2a is the spectrum recorded after the first TEOS exposure of 5.1×10^8 L at 300 K with 5 Torr of NH_3 referenced to the spectrum recorded prior to the TEOS exposure. This TEOS exposure was defined by a TEOS pressure of 0.85 Torr for 10 min.

The spectrum in Fig. 2a reveals a negative absorbance feature in the O-H stretching region with peaks at 3680 and 3730 cm^{-1}. Positive absorbance features are also observed in the C-H stretching region with peaks at 2901, 2933, and 2979 cm^{-1}. These observed changes in the spectrum shown in Fig. 2a are consistent with TEOS reacting with the hydroxyl groups on the $BaTiO_3$ particles as described by Eq. 4. Based on the gas-phase vibrational spectrum of TEOS, the C-H stretches observed at 2901, 2933, and 2979 cm^{-1} are expected from $Si(OCH_2CH_3)_x$* surface species.[25]

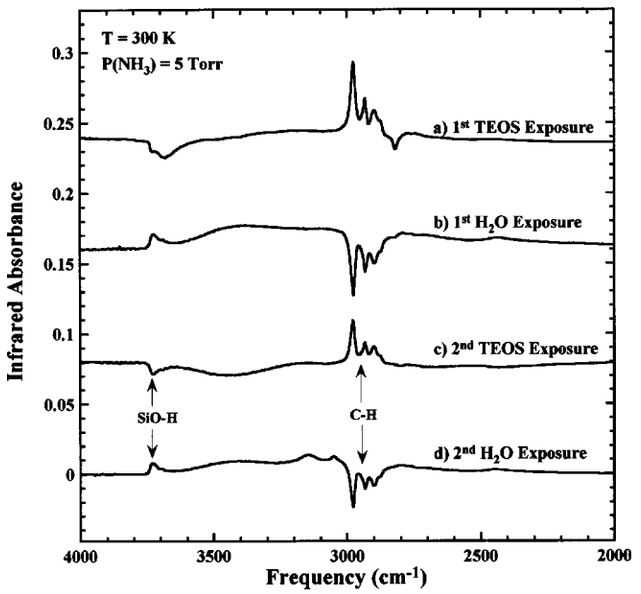

Figure 2. FTIR difference spectra of the $BaTiO_3$ particles in the O-H, N-H, and C-H stretching regions after the (a) 1st TEOS exposure, (b) 1st H_2O exposure, (c) 2nd TEOS exposure, and (d) 2nd H_2O exposure. All the exposures were performed at 300 K with 5 Torr NH_3.

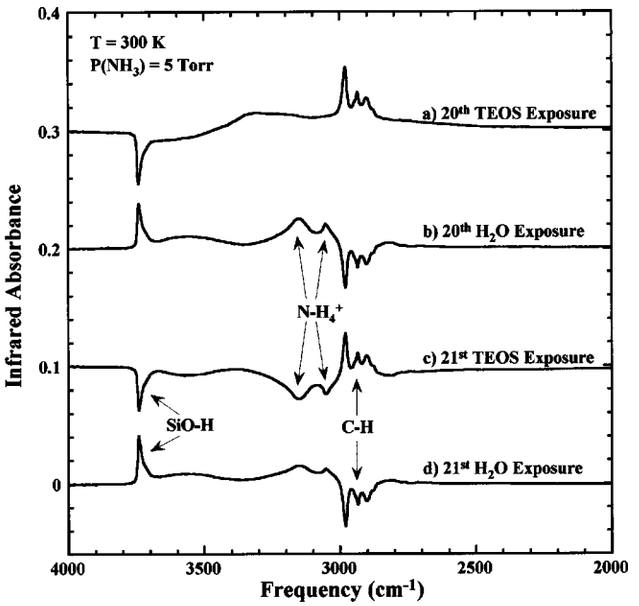

Figure 3. FTIR difference spectra of the $BaTiO_3$ particles in the O-H, N-H, and C-H stretching regions after the (a) 20th TEOS exposure, (b) 20th H_2O exposure, (c) 21st TEOS exposure, and (d) 21st H_2O exposure. All the exposures were performed at 300 K with 5 Torr NH_3.

A small negative absorbance feature also appears in Fig. 2a in the C-H stretching region at ~2820 cm^{-1}. This feature results from the partial removal of some hydrocarbon contamination on the initial $BaTiO_3$ particles. Absorbance features from these C-H stretching vibrations are observed in the FTIR spectrum of the initial $BaTiO_3$ particles shown in Fig. 1.

Figure 2b shows the difference spectrum recorded after the subsequent H_2O exposure of 4.1×10^{10} L at 300 K with 5 Torr NH_3. This H_2O exposure was defined by an H_2O pressure of 5.0 Torr for 15 min followed by an H_2O pressure of 10.0 Torr for 60 min. The spectrum reveals a positive absorbance feature in the O-H stretching region with a peak at 3726 cm^{-1}. Additionally, negative absorbance features are observed at 2901, 2933, and 2979 cm^{-1}. This spectrum is consistent with H_2O reacting with $Si(OCH_2CH_3)$* species to form SiOH* species according to Eq. 4. Figures 2c and d show the evolution of the difference spectra during the 2nd TEOS and H_2O exposures at 300 K with 5 Torr of NH_3.

The difference spectra after the TEOS and H_2O exposures of 3.6×10^9 L and 3.6×10^{10} L, respectively, at 300 K with NH_3 at 5 Torr during the 20th and 21st AB cycles are shown in Fig. 3. The difference spectra shown in Fig. 3a and c are similar and have negative absorbance features at 3743 cm^{-1}, corresponding to a SiO-H stretching vibrational mode. The positive absorbance features at 2901, 2933, and 2979 cm^{-1} correspond to the C-H stretching vibrations of $Si(OCH_2CH_3)_x$* species.[25] Figure 3b and d reveal difference spectra that are nearly identical to each other but mirror images of Fig. 3a and c. The spectra are consistent with the sequential exposures of TEOS and H_2O yielding $Si(OCH_2CH_3)$* and SiOH* species, respectively.

Some of the spectra in Fig. 2 and 3 display a broad absorption in the range from 3200 to 3500 cm^{-1}. More distinct absorption features are also observed at 3050 and 3150 cm^{-1}. These features are attributed to adsorbed NH_3 species. These adsorbed NH_3 species are removed during long evacuations or mild anneals. The broad absorption feature in the range from 3200 to 3500 cm^{-1} is similar to the spectrum of liquid NH_3[26] and is attributed to a liquid-like NH_3 layer. Additionally, the features at 3050 and 3150 cm^{-1} are assigned to the $(\upsilon_2 + \upsilon_4)$ and υ_3 vibrational modes of the ammonium ion (NH_4^+), respectively.[11,27,28]

Figure 4 illustrates that the NH_4^+ species are removed after long pumpouts. Figure 4a shows a spectrum recorded shortly after the H_2O exposure of 8.5×10^{10} L with an NH_3 pressure of 5 Torr during the 15th cycle. Figure 4b displays the subsequent spectrum taken after a pumpout of several days at room temperature. The difference spectrum in Fig. 4c shows the changes that occurred dur-

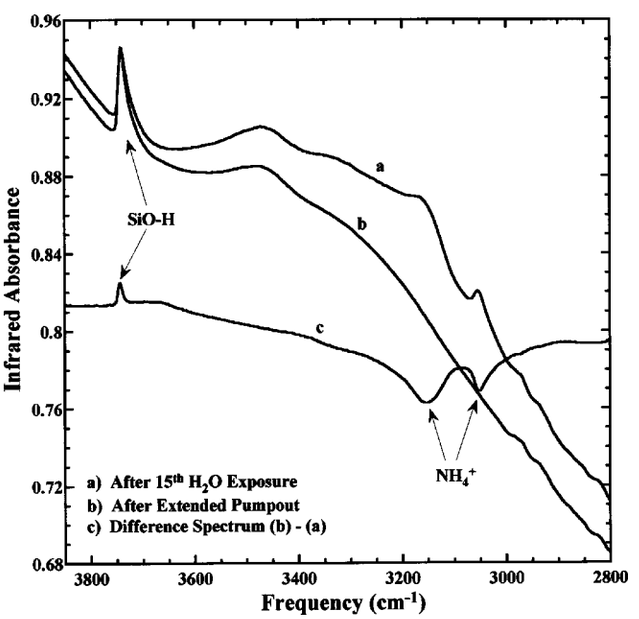

Figure 4. (a) FTIR spectrum recorded shortly after the 15th H_2O exposure with an NH_3 pressure of 5 Torr. (b) Subsequent FTIR spectrum recorded after room temperature pumpout for several days. (c) FTIR difference spectrum (b-a).

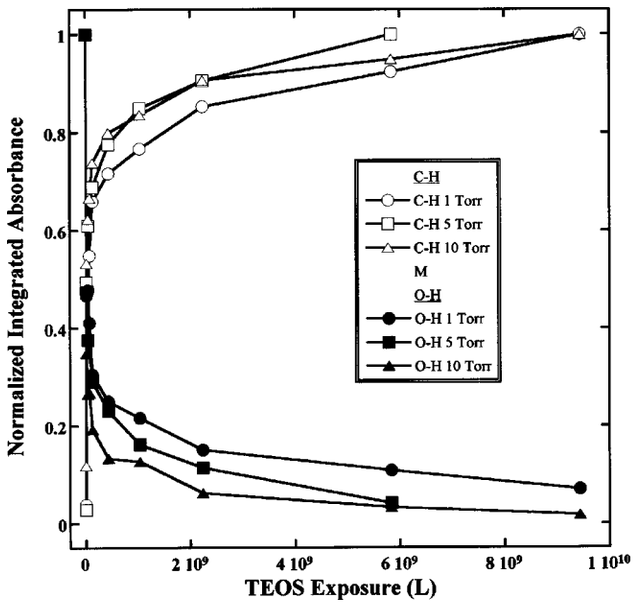

Figure 5. Normalized integrated absorbance of the (●, ■, ▲) O-H and (○, □, △) C-H stretching regions *vs.* TEOS exposure at 300 K and NH_3 pressures of 1, 5, and 10 Torr.

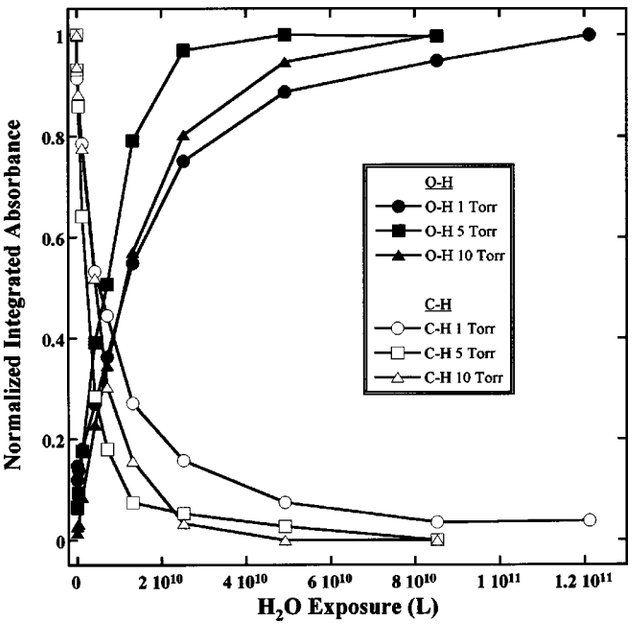

Figure 6. Normalized integrated absorbance of the (●, ■, ▲) O-H and (○, □, △) C-H stretching regions *vs.* H_2O exposure at 300 K and NH_3 pressures of 1, 5, and 10 Torr.

ing the long pumpout. The negative features at 3050 and 3150 cm^{-1} in the difference spectrum correspond to the loss of NH_4^+ species. Concurrently, the positive feature at 3741 cm^{-1} corresponds to the growth of SiOH* species.[6,8,29] The loss of NH_4^+ species and the simultaneous growth of SiOH* surface species is explained by the following reaction

$$SiO^- + NH_4^+ \rightarrow SiOH^* + NH_3 \qquad [5]$$

The NH_4^+ species transfers a proton to the SiO^- surface species to form SiOH*. The proton transfer is then followed by NH_3 desorption from the SiO_2 surface.

The NH_4^+ species were also observed after the TEOS exposure of 5.8×10^9 L with an NH_3 pressure of 5 Torr during the 15th cycle. The NH_4^+ species were also removed after long pumpouts. The intensities of the peaks at 3050 and 3150 cm^{-1} were less after this TEOS exposure of 5.8×10^9 L than after the previous H_2O exposure of 8.5×10^{10} L. The features corresponding to the NH_4^+ species were only observed after the TEOS and H_2O exposures during the 15th, 16th, and 19th AB cycles. This behavior is attributed to the much longer reactant exposures that were used during these particular reaction cycles.

The effect of NH_3 pressure on the TEOS and H_2O reactions was also investigated at 300 K. At various NH_3 pressures, the integrated absorbances of the SiO-H stretching vibrations and the C-H stretching vibrations were examined *vs.* TEOS and H_2O exposures. Reactive uptakes were obtained for NH_3 pressures of 1, 5, and 10 Torr during the 16th, 15th, and 19th AB cycles, respectively.

Figure 5 displays the normalized integrated absorbances during the TEOS reaction described by Eq. 3. With increasing TEOS exposure using TEOS pressures between 0.2 and 1.0 Torr, the integrated absorbance of the O-H feature decreases and the integrated absorbance of the C-H features increases before leveling off. With NH_3 pressures of 5 and 10 Torr, the TEOS reacts nearly completely with the SiOH* species after a TEOS exposure of 6×10^9 L. With only 1 Torr of NH_3, the TEOS has not completely reacted with the SiOH* species after an exposure of 9.4×10^9 L.

The normalized integrated absorbances during the H_2O reaction described by Eq. 4 are displayed in Fig. 6. With increasing H_2O exposure using H_2O pressures between 1.0 and 10 Torr, the integrated absorbance of the O-H feature increases and the integrated absorbance of the C-H features decreases before leveling off. Similar to the TEOS reaction, NH_3 pressures of 5 and 10 Torr were sufficient for the H_2O reaction to proceed to near completion. With 5 and 10 Torr of NH_3, the $Si(OCH_2CH_3)$* species were almost entirely removed after an H_2O exposure of $\sim 8.5 \times 10^{10}$ L. An exposure of 1.2×10^{11} L was not sufficient to deplete all of the $Si(OCH_2CH_3)$* species when the NH_3 pressure was only 1 Torr.

Additional FTIR experiments were conducted to investigate the necessity of the NH_3 catalyst for the TEOS and H_2O reactions. A spectrum (I) was recorded after nine AB cycles ending with a H_2O/NH_3 exposure. The H_2O exposure was 1.1×10^{11} L and the NH_3 pressure was 10 Torr. Another spectrum (II) was recorded after only a TEOS exposure of 4.5×10^9 L during the 10th AB cycle followed by an 8 h evacuation time. Figure 7a shows the difference spectrum (II − I). Without the NH_3 catalyst, only minimal changes are present in the FTIR spectra. The long evacuation time of 8 h was necessary to remove hydrogen-bonded NH_3 species from the surface.

Spectrum (III) was recorded after a subsequent TEOS exposure of 7.2×10^9 L with 5-10 Torr of NH_3. The difference spectrum (III-I) shown in Fig. 7b reveals the loss of an SiO-H stretching feature and the gain of C-H vibrational features at 2901, 2933, and 2979 cm^{-1}. Additional positive features are observed at frequencies of 970, 1086, 1109, 1170, 1298, 1369, 1394, 1447, and 1484 cm^{-1}. All these positive features are similar in frequency to the various vibrational modes in the infrared spectrum of molecular TEOS.[25] These positive features are expected from the reaction of TEOS with SiOH* surface species to form $Si(OCH_2CH_3)_x$* surface species.

Experiments were also conducted to illustrate the importance of NH_3 for the H_2O reaction. Spectrum (IV) was recorded after 9.5 AB cycles ending with a TEOS/NH_3 exposure. The TEOS exposure was 7.2×10^9 L and the NH_3 pressure was between 5 and 10 Torr. Another spectrum (V) was recorded after only an H_2O exposure of

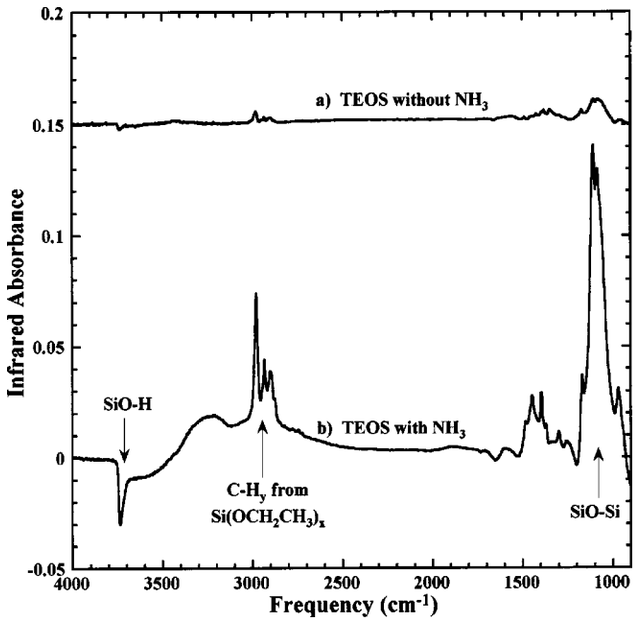

Figure 7. FTIR difference spectra of the $BaTiO_3$ particles during the 10th cycle TEOS exposures. (a) Spectrum recorded after a TEOS exposure without NH_3 followed by an 8 h evacuation. (b) Spectrum recorded after a subsequent TEOS exposure with 5-10 Torr NH_3. The reference spectrum was recorded after nine AB cycles ending with an H_2O/NH_3 exposure.

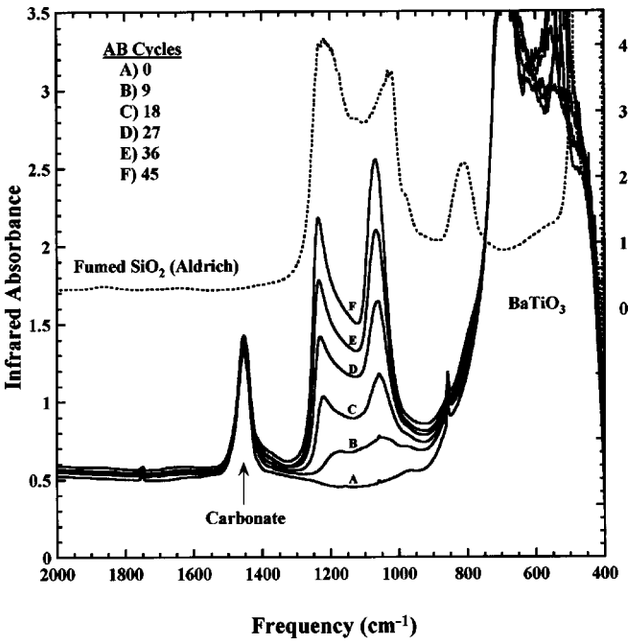

Figure 9. FTIR spectra displaying the progressive growth of SiO_2 bulk vibrational modes. The spectra were recorded after various numbers of AB cycles at 300 K after the H_2O/NH_3 exposure. The spectrum of fumed SiO_2 particles is shown for comparison.

2.2×10^9 L during the 10th AB cycle followed by a 10 h evacuation time. Figure 8a shows the difference spectrum (V-IV). The changes in the O-H and C-H stretching regions are minimal without the NH_3 catalyst. Spectrum (VI) was recorded after a subsequent H_2O exposure of 5.4×10^{10} L with 10 Torr of NH_3. The difference spectrum (VI-IV) shown in Fig. 8b reveals the gain of an SiO-H stretching feature and the loss of features associated with $Si(OCH_2CH_3)_x$* surface species. These changes are expected from the reaction of H_2O with $Si(OCH_2CH_3)_x$* surface species to form SiOH* surface species.

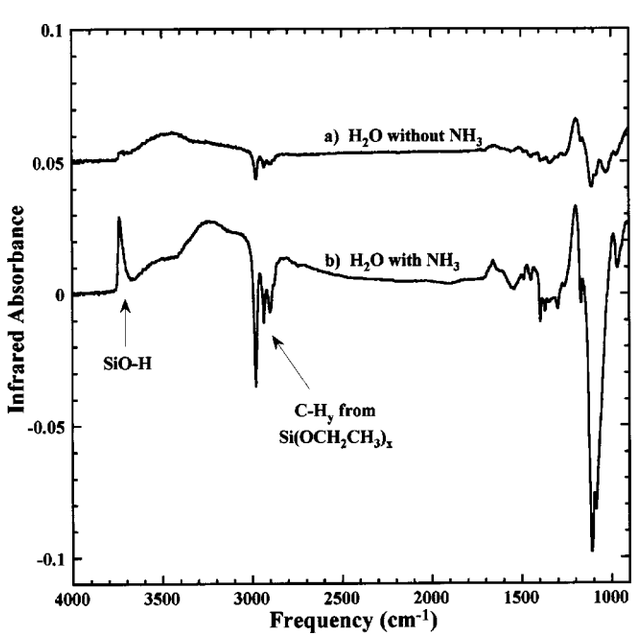

Figure 8. FTIR difference spectra of the $BaTiO_3$ particles during the 10th cycle H_2O exposures. (a) Spectrum recorded after a H_2O exposure without NH_3 followed by an 8 h evacuation. (b) Spectrum recorded after a subsequent H_2O exposure with 10 Torr NH_3. The reference spectrum was recorded after 9.5 AB cycles ending with a $TEOS/NH_3$ exposure.

Film growth.—The results in the previous section reveal that the NH_3 catalyst is necessary for the TEOS and H_2O reactions. The results indicate that an NH_3 pressure of 5 Torr is sufficient to catalyze the TEOS and H_2O reactions. All AB cycles for catalyzed SiO_2 ALD growth on the $BaTiO_3$ particles used an NH_3 pressure of 5 Torr except the 16th (1 Torr) and 19th (10 Torr) cycles. Typical exposures consisted of 1 Torr of TEOS or 10 Torr of H_2O for 60 min each. During $TEOS/NH_3$ exposures, the TEOS was introduced into the chamber before the NH_3 because of the relatively low vapor pressure of TEOS. During H_2O/NH_3 exposures, the NH_3 was introduced into the chamber before the H_2O.

FTIR spectroscopy monitored the growth of SiO_2 on the $BaTiO_3$ particles during the 45 NH_3-catalyzed $TEOS/H_2O$ reaction cycles at 300 K. Figure 9 shows the infrared spectra in the SiO_2 bulk vibrational region after the H_2O exposures during the $TEOS/H_2O$ reaction cycles. All the spectra reveal the strong $BaTiO_3$ absorption below $\sim$750 cm^{-1} and the carbonate peak at $\sim$1450 cm^{-1}. SiO_2 growth *vs.* number of AB cycles is observed in the region from 1000-1250 cm^{-1} and corresponds to the bulk vibrational mode of SiO_2.[30]

The SiO_2 absorbance feature in the region from 1000 to 1250 cm^{-1} has peaks at $\sim$1070 and $\sim$1235 cm^{-1}. These features are similar in frequency to features that appear in infrared studies of thin SiO_2 films. These investigations observe a transverse-optical (TO) phonon mode at 1075 cm^{-1} and a longitudinal-optical (LO) phonon mode at 1250 cm^{-1}.[31] For comparison, a spectrum of fumed SiO_2 particles is also displayed in Fig. 9. The fumed SiO_2 particles (Aldrich Chemical Company) had a surface area of 380 m^2/g and an average diameter of 70 Å. The features observed in the spectrum of the fumed SiO_2 particles are similar to the SiO_2 features that are

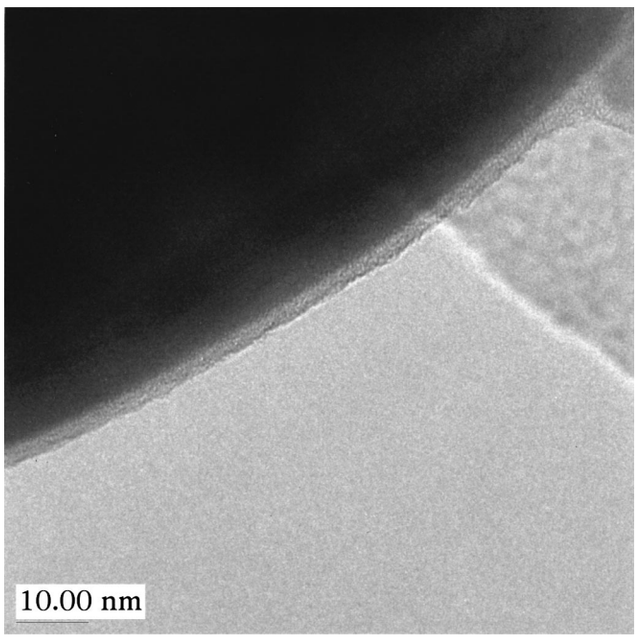

Figure 10. TEM image of $BaTiO_3$ particle coated by catalyzed SiO_2 ALD with a thickness of ~35 Å after 45 AB cycles at 300 K.

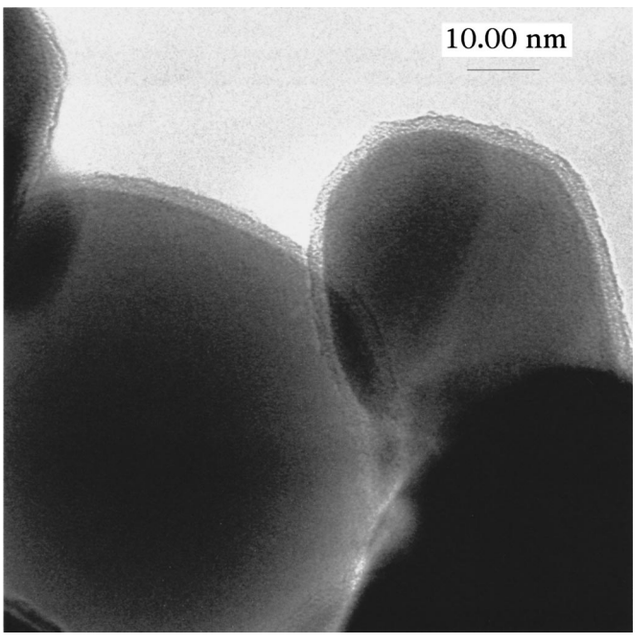

Figure 12. TEM images of ZrO_2 particles coated by catalyzed SiO_2 ALD with a thickness of ~25 Å after 35 AB cycles at 300 K.

progressively growing on the $BaTiO_3$ particles with increasing number of AB reaction cycles.

The SiO_2 deposition on the $BaTiO_3$ particles was also evaluated using TEM. A TEM image of an SiO_2-coated $BaTiO_3$ particle is shown in Fig. 10. The SiO_2 film was deposited by 45 AB cycles at 300 K with the NH_3 catalyst at a pressure of 5 Torr. These were the same 45 AB reaction cycles employed in the transmission FTIR studies. Figure 11 shows a TEM image recorded after the 45 AB cycles and an anneal in vacuum to 1100 K.

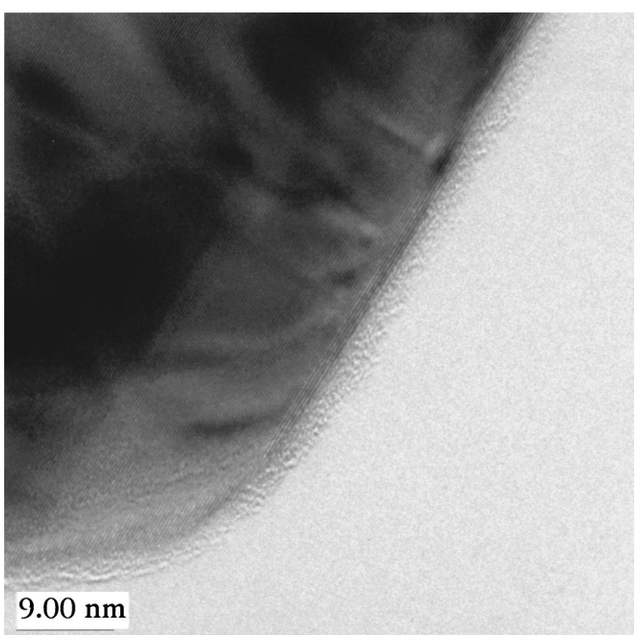

Figure 11. TEM image of $BaTiO_3$ particle coated by catalyzed SiO_2 ALD with a thickness of ~35 Å after 45 AB cycles at 300 K followed by a vacuum anneal at 1100 K.

Both TEM images in Fig. 10 and 11 reveal a coating that is uniform and conformal to the underlying $BaTiO_3$ surface. Figure 11 reveals a crystalline $BaTiO_3$ particle and an amorphous SiO_2 ALD film. Film thicknesses obtained from Fig. 10 and 11 and additional TEM images not shown reveal a coating on the $BaTiO_3$ particles of ~35 Å. The vacuum anneal at 1100 K did not have a significant effect on the thickness of the coatings. The SiO_2 film thickness after 45 AB cycles yields an SiO_2 ALD growth rate of ~0.8 Å per AB cycle.

Similar results were obtained on the ZrO_2 particles. A TEM image of SiO_2-coated ZrO_2 particles is shown in Fig. 12. This SiO_2 film was deposited using 35 AB cycles at 300 K with the NH_3 catalyst pressure at 5 Torr. The typical exposures used during the SiO_2 deposition on the ZrO_2 particles were 2.5×10^9 and 1.8×10^{10} L for the TEOS and H_2O exposures, respectively. The TEM image reveals that the SiO_2 coating is uniform and conformal to the underlying ZrO_2 surface. The TEM images of the SiO_2-coated ZrO_2 particles reveal a film coating of ~25 Å. This SiO_2 thickness after 35 AB cycles is consistent with an SiO_2 ALD growth rate of ~0.7 Å per AB cycle.

Catalysis mechanism.—NH_3 is an effective catalyst for SiO_2 ALD. To explore the catalysis mechanism, the FTIR spectra of NH_3 adsorbed on the hydroxylated SiO_2 surface was examined under isothermal and isobaric conditions. Figure 13 shows some of the spectra of the SiO_2 particles *vs.* NH_3 pressure at 300 K. The absorption peak at 3746 cm^{-1} represents the O-H stretching vibration of the isolated SiOH* hydroxyl species.[6,8,29] The broad peak centered at around 2970 cm^{-1} represents the SiOH* hydroxyl species that have been red-shifted by hydrogen-bonding with adsorbed NH_3.[32] The isolated hydroxyl peak decreases as the hydrogen-bonded hydroxyl peak increases with increasing NH_3 pressure at 300 K.

Figure 13 also reveals features associated with adsorbed NH_3 molecules. The absorption peaks at 3320 and 3400 cm^{-1} represent the symmetric and asymmetric NH_3 stretches, respectively.[33,34] The spectra at lower frequencies also display a corresponding absorption by a NH_3 scissors vibration at 1634 cm^{-1} that is consistent with

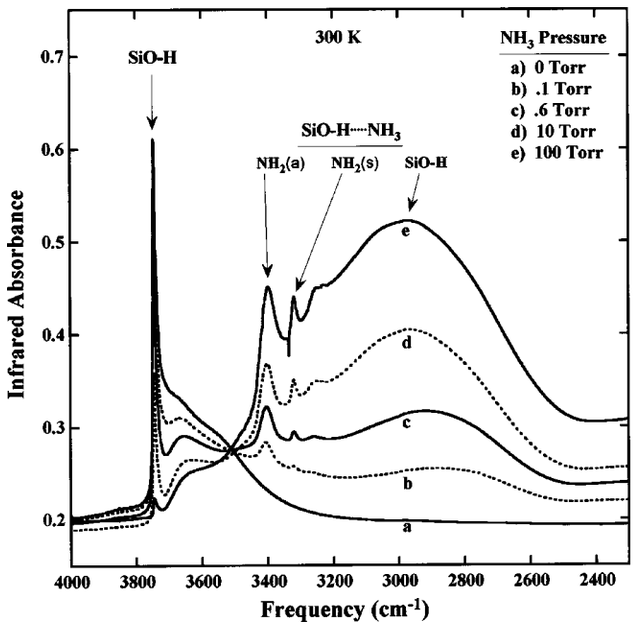

Figure 13. FTIR spectra of (a) hydroxylated SiO_2 particles in vacuum and the hydroxylated SiO_2 particles with NH_3 pressures of (b) 0.1, (c) 0.6, (d) 10, and (e) 100 Torr. All the spectra were recorded at 300 K.

adsorbed NH_3. All three of these NH_3 features grow with increasing NH_3 pressure at constant temperature.

FTIR spectra of NH_3 were also recorded on the hydroxylated SiO_2 surface *vs.* temperature at a constant NH_3 pressure of 5 Torr. Some of these spectra are shown in Fig. 14. The NH_3 stretching peaks at 3320 and 3400 cm^{-1} and the hydrogen-bonded hydroxyl peak centered around 2970 cm^{-1} decrease with increasing temperature. This decrease is attributed to larger NH_3 desorption rates at higher temperature. The isolated hydroxyl peak at 3746 cm^{-1} concurrently reappears at higher temperature with the disappearance of NH_3 and hydrogen-bonded SiOH* features.

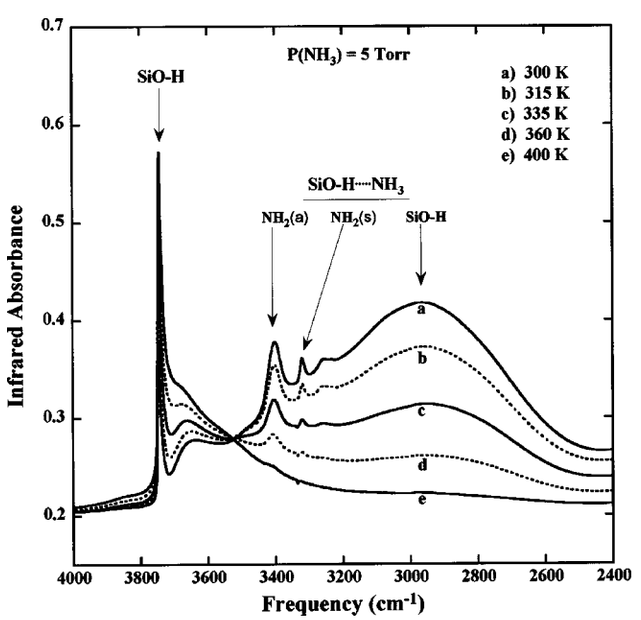

Figure 14. FTIR spectra of hydroxylated SiO_2 particles with an NH_3 pressure of 5 Torr recorded at temperatures of (a) 300, (b) 315, (c) 335, (d) 360, and (e) 400 K.

The FTIR spectra of NH_3 adsorbed on hydroxylated SiO_2 under isothermal and isobaric conditions reveal the strong hydrogen-bonding interaction of NH_3 with SiOH* surface hydroxyl groups. Figure 13 reveals that hydrogen bonding substantially weakens the O-H bond and shifts the O-H stretching frequency to lower frequencies. This hydrogen bonding also makes the oxygen in SiOH* a stronger nucleophile for chemical attack on the TEOS silicon precursor.[35] This enhancement of the nucleophilicity of oxygen is believed to be the primary catalytic effect of NH_3.

The temperature-dependent results for NH_3 adsorption on hydroxylated SiO_2 under isobaric conditions indicate the delicate balance between NH_3 adsorption and NH_3 desorption rates. Figure 14 indicates that an NH_3 pressure of 5 Torr at 300 K is sufficient for NH_3 adsorption on nearly all the SiOH* surface species. At progressively higher temperatures, larger NH_3 desorption rates decrease the amount of NH_3 adsorbed on SiOH* surface species. The catalytic effect of NH_3 should decrease with the reduction of adsorbed NH_3. In agreement with this expectation, a dramatic temperature dependence for catalytic SiO_2 ALD has been observed in earlier studies.[9,10]

NH_3 is necessary for both the TEOS and H_2O reactions during catalytic SiO_2 ALD. Figures 13 and 14 illustrate the effect of NH_3 on the SiOH* surface species that react with TEOS. Similar interactions may occur between NH_3 and the H_2O reactant during the H_2O reaction. In this case, NH_3 would hydrogen bond with adsorbed H_2O on the SiO_2 surface. This hydrogen bonding would make the oxygen in H_2O a stronger nucleophile for chemical attack on $SiOCH_2CH_3$* surface species.

Both Fig. 13 and 14 reveal a distinct isobestic point where the infrared absorbance of the spectra does not change *vs.* pressure under isothermal conditions or *vs.* temperature under isobaric conditions. These isobestic points are observed at 3510 cm^{-1} in Fig. 13 and 3520 cm^{-1} in Fig. 14. Isobestic points occur when a composite spectrum is a combination of two separate states, *e.g.*, X and Y, with distinct spectra. The composite spectrum is either 100% X, 100% Y, or some combination of X and Y totaling 100%, *e.g.*, 60% X and 40% Y. The isobestic point is the frequency where the spectrum for 100% X and 100% Y have the same absorbance. At this isobestic frequency, changes in the combination of the two separate states will not alter the absorbance.

The isobestic points establish the one-to-one relationship between the loss of isolated SiOH* surface species (X) and gain of hydrogen-bonded SiOH* surface species (Y). NH_3 interacts with individual SiOH* surface species without perturbing neighboring SiOH* surface species. The composite spectrum is just a combination of % X and % Y. No evidence exists for any NH_3 interactions between surface sites because there is no additional NH_3 coverage dependence. Given the distinct isobestic points, the catalytic effect of NH_3 is expected to be linear with adsorbed NH_3 coverage.

Conclusions

SiO_2 ALD was accomplished at room temperature with TEOS and H_2O using NH_3 as the catalyst. The use of TEOS instead of chlorosilanes as the silicon precursor avoids the production of HCl reaction products. HCl can react with the NH_3 catalyst to produce $NH_4^+Cl^-$ salt that impedes the SiO_2 film growth. Sequential exposures of TEOS and H_2O at 300 K with 5 Torr of NH_3 led to SiO_2 ALD on $BaTiO_3$ and ZrO_2 particles. FTIR spectroscopy monitored the surface reactions *vs.* TEOS/H_2O reaction cycles during SiO_2 ALD. TEOS reacted with the SiOH* surface species and formed $Si(OCH_2CH_3)$* surface species. Subsequent H_2O exposures led to the formation SiOH* species and removal of $Si(OCH_2CH_3)$* spe-

cies. Monitoring the TEOS and H_2O reactions with varying NH_3 pressures demonstrated that an NH_3 pressure of 5 Torr was effective to catalyze SiO_2 ALD at 300 K.

Sequential TEOS and H_2O exposures at 300 K led to progressive SiO_2 growth. FTIR studies observed the SiO_2 growth by monitoring the SiO_2 bulk vibrational modes that increased progressively with each TEOS and H_2O exposure. The SiO_2 deposition was also revealed by TEM images of the SiO_2-coated $BaTiO_3$ and ZrO_2 particles. On the $BaTiO_3$ particles, 45 TEOS/H_2O reaction cycles at 300 K yielded conformal SiO_2 films with thicknesses of ~35 Å. Conformal SiO_2 films with thicknesses of ~25 Å were observed after 35 TEOS/H_2O reaction cycles at 300 K on the ZrO_2 particles. These SiO_2 thicknesses yielded an SiO_2 ALD growth rate of 0.7-0.8 Å/AB cycle at 300 K. The TEM images revealed that the SiO_2 ALD coatings were amorphous on the underlying crystalline $BaTiO_3$ and ZrO_2 particles.

The NH_3 catalytic mechanism was investigated by monitoring the effect of NH_3 on the FTIR spectra of hydroxylated SiO_2 surfaces under isothermal and isobaric conditions. Adsorbed NH_3 removed the isolated SiOH* surface species and produced significantly red-shifted hydrogen-bonded SiOH* surface species. The catalytic mechanism is linked to the enhanced nucleophilic character of oxygen in the perturbed SiOH* surface species. Isobestic points were observed in the FTIR spectra *vs.* NH_3 pressure at constant temperature and *vs.* temperature at constant NH_3 pressure. These isobestic points are consistent with a one-to-one relationship between the loss of isolated SiOH* surface species and gain of hydrogen-bonded SiOH* surface species.

Acknowledgments

This research was partially supported by the Center for Composite and Ceramic Materials at the University of New Mexico. Additional support was obtained from the National Science Foundation (NSF) through grant no. CHE-9905812. E.R.S. also acknowledges support from the NSF Research Experience for Undergraduates (REU) program in the Department of Chemistry and Biochemistry at the University of Colorado.

The University of Colorado assisted in meeting the publication costs of this article.

References

1. T. Suntola, *Thin Solid Films*, **216**, 84 (1992).
2. S. M. George, A. W. Ott, and J. W. Klaus, *J. Phys. Chem.*, **100**, 13121 (1996).
3. M. Ritala and M. Leskela, in *Handbook of Thin Film Materials*, H. S. Nalwa, Editor, p. 103, Academic Press, San Diego (2001).
4. S. M. Rossnagel, A. Sherman, and F. Turner, *J. Vac. Sci. Technol. B*, **18**, 2016 (2000).
5. D. J. Ehrlich and J. Melngailis, *Appl. Phys. Lett.*, **58**, 2675 (1991).
6. O. Sneh, M. L. Wise, A. W. Ott, L. A. Okada, and S. M. George, *Surf. Sci.*, **334**, 135 (1995).
7. J. W. Klaus, A. W. Ott, J. M. Johnson, and S. M. George, *Appl. Phys. Lett.*, **70**, 1092 (1997).
8. J. D. Ferguson, A. W. Weimer, and S. M. George, *Chem. Mater.*, **12**, 3472 (2000).
9. J. W. Klaus, O. Sneh, and S. M. George, *Science*, **278**, 1934 (1997).
10. J. W. Klaus and S. M. George, *Surf. Sci.*, **447**, 81 (2000).
11. C. P. Tripp, P. Kazmaier, and M. L. Hair, *Langmuir*, **12**, 6407 (1996).
12. M. Muroyama, A. Kawashima, and J. Sato, *Jpn. J. Appl. Phys., Part 1*, **32**, 6122 (1993).
13. J. E. Crowell, L. L. Tedder, H. C. Cho, F. M. Cascarano, and M. A. Logan, *J. Vac. Sci. Technol. A*, **8**, 1864 (1990).
14. E. J. Kim and W. N. Gill, *J. Electrochem. Soc.*, **142**, 676 (1995).
15. J. P. Blitz, R. S. S. Murthy, and D. E. Leyden, *J. Colloid Interface Sci.*, **126**, 387 (1988).
16. G. R. Bogart and D. E. Leyden, *J. Colloid Interface Sci.*, **167**, 27 (1994).
17. J. D. Ferguson, A. W. Weimer, and S. M. George, *Thin Solid Films*, **371**, 95 (2000).
18. J. D. Ferguson, A. W. Weimer, and S. M. George, *Thin Solid Films*, **413**, 16 (2002).
19. T. H. Ballinger, J. C. S. Wong, and J. T. Yates, *Langmuir*, **8**, 1676 (1992).
20. M. D. B. Lopez, G. Fourlaris, B. Rand, and F. L. Riley, *J. Am. Ceram. Soc.*, **82**, 1777 (1999).
21. S. W. Lu, B. I. Lee, and L. A. Mann, *Mater. Lett.*, **43**, 102 (2000).
22. J. D. Ferguson, A. R. Yoder, A. W. Weimer, and S. M. George, *Appl. Surf. Sci.*, **226**, 393 (2004).
23. M. Primet, P. Pichat, and M.-V. Mathieu, *J. Phys. Chem.*, **75**, 1216 (1971).
24. T. Noma, S. Wada, M. Yano, and T. Suzuki, *J. Appl. Phys.*, **80**, 5223 (1996).
25. M. A. Mondragon, V. M. Castano, J. Garcia, and C. A. Tellez, *Vib. Spectrosc.*, **9**, 293 (1995).
26. J. C. Dougal, P. Gans, and J. B. Gill, *J. Chem. Soc., Faraday Trans. 1*, **84**, 657 (1988).
27. M. J. D. Low, A. G. Severdia, and J. Chan, *J. Catal.*, **71**, 144 (1981).
28. P. Van der Voort, K. C. Vrancken, and E. F. Vansant, *J. Chem. Soc., Faraday Trans.*, **89**, 2509 (1993).
29. F. Boccuzzi, S. Coluccia, G. Ghiotti, C. Morterra, and A. Zecchina, *J. Phys. Chem.*, **82**, 1298 (1978).
30. *Infrared Spectra of Inorganic Compounds*, Vol. IV., R. A. Nyquist and R. O. Kagel, Editors, Vol. IV, Academic Press, Inc., London (1997).
31. C. H. Bjorkman, T. Yamazaki, S. Miyazaki, and M. Hirose, *J. Appl. Phys.*, **77**, 313 (1995).
32. G. Curthoys, V. Y. Davydov, A. V. Kiselev, S. A. Kiselev, and B. V. Kuznetso, *J. Colloid Interface Sci.*, **48**, 58 (1974).
33. M. L. Hair and W. Hertl, *J. Phys. Chem.*, **73**, 4269 (1969).
34. A. A. Tsyganenko, D. V. Pozdnyakov, and V. N. Filimonov, *J. Mol. Struct.*, **29**, 299 (1975).
35. C. P. Tripp and M. L. Hair, *J. Phys. Chem.*, **97**, 5693 (1993).